

China's first step towards probing the expanding universe and the nature of gravity using a space borne gravitational wave antenna

The Taiji Scientific Collaboration*

In this perspective, we outline that a space borne gravitational wave detector network combining LISA and Taiji can be used to measure the Hubble constant with an uncertainty less than 0.5% in ten years, compared with the network of the ground based gravitational wave detectors which can measure the Hubble constant within a 2% uncertainty in the next five years by the standard siren method. Taiji is a Chinese space borne gravitational wave detection mission planned for launch in the early 2030 s. The pilot satellite mission Taiji-1 has been launched in August 2019 to verify the feasibility of Taiji. The results of a few technologies tested on Taiji-1 are presented in this paper.

The observation of gravitational waves (GWs) enables us to explore the Universe in more details than that is currently known. By testing the theory of general relativity, it can unveil the nature of gravity. In particular, a GW can be used to determine the Hubble constant by a standard siren method^{1,2}. This method³ was first used by the Advanced LIGO⁴ and Virgo⁵ observatories when they discovered GW event GW170817⁶. Despite the degeneracy problem in the ground-based GW detectors, the Hubble constant can reach a precision of 2% after a 5-year observation with the network of the current surface GW detectors⁶, although LIGO's O3 data have shown that the chance to detect electromagnetic (EM) counterpart might be a little optimistic⁷.

In this paper, we discuss a method to further improve the fractional uncertainty of the Hubble constant to a precision <1% by the space-borne GW antennas. The improvement not only comes from that a space-borne GW antenna such LISA^{8,9} and Taiji^{10–13} can avoid the degeneracy problem because of its orbital motion¹⁴ but also the precision of a GW source's position and its luminosity distance can be improved by 2–3 orders of magnitude by the LISA–Taiji network¹⁵, compared to the individual antenna such as LISA or Taiji. It requires a 1-year overlap of LISA and Taiji missions to achieve this precision.

The joint measurement requires that the Taiji scientific collaboration establish a three-step plan to guarantee the launch of Taiji in the 2030s¹³. The first step of this new observatory is to launch a pilot satellite, Taiji-1, to prepare the necessary technology for the second step, Taiji pathfinder, also called Taiji-2. Consisting of two satellites, Taiji-2 will be used to demonstrate the Taiji technology around 2023–2025.

Launched in 2019, Taiji-1 accomplished multiple tasks^{12,13}. It studied the manufacturing process for the Taiji payload, the on-orbital working sequence of the Taiji payload, the data processing stream for the Taiji mission, and the feasibility of a few Taiji key technologies in space. In this article, we will also report the main results of the payload test for Taiji-1.

The Hubble constant and the standard siren method

By observing the redshift of a specific spectral line of a remote galaxy, it has been found that the further away a galaxy is from us, the faster it appears to recede¹⁶. This observation is known as

*A list of authors and their affiliations appears at the end of the paper.

Hubble’s law

$$V_H = H_0 \cdot d \tag{1}$$

Hubble’s law is interpreted as an evidence that the universe has been expanding since the Big Bang occurred ~13.8 billion years ago¹⁷. In Eq. 1, H_0 is the mean expansion rate of the Universe, called the Hubble constant, V_H is the receding velocity of the galaxy, and d is the distance of the receding galaxy. According to the Friedmann–Robertson–Walker cosmological model (FRW model), the dynamics of our expanding universe are governed by the density and the curvature of our universe. By measuring the Hubble constant, one can deduce the age, the size, the current state, and even the fate of our Universe¹⁸. In general, there are two primary methods to measure the Hubble constant. The first way to estimate the distance is to exploit the so-called “standard candles”—Cepheid variable stars or type 1a supernovae that are at the same luminosity. The data from the first method¹⁹ implies that the value of $H_0 = (74.03 \pm 1.42) \text{ km s}^{-1} \text{ Mpc}^{-1}$ at 68% confidence level. The other method focuses on the cosmic microwave background, and it examines how the cosmic microwave background has evolved over time. The data from the cosmic microwave background²⁰ indicates that the value of $H_0 = (67.4 \pm 0.5) \text{ km s}^{-1} \text{ Mpc}^{-1}$ at 68% confidence level. The mismatch between the two measurements needs to be explained since the values should agree if the models are correct.

A new and independent determination of the Hubble constant using a GW as a standard siren^{1,2} may solve this cosmic riddle. In 2017, the Advanced LIGO and Virgo detectors observed a GW signal (event GW170817) from the merger of a binary neutron-star system²¹. The EM follow-up measurements of the area were then sequentially observed, which triggered the first “multi-messenger” astronomical observation²². With the absolute distance to the source being determined directly from the GW measurements, GW170817 was used as a “standard siren” to measure the Hubble constant⁵. The Hubble constant was found in this case to be $70.0_{-8.0}^{+12.0} \text{ km s}^{-1} \text{ Mpc}^{-1}$. The uncertainty in the Hubble constant measurement (Eq. 1) largely comes from the inaccuracy of the absolute distance evaluation. The receding velocity, represented by a galaxy’s redshift, can be measured precisely by taking the spectra of the galaxy. For a ground-based GW observatory, such as the LIGO and Virgo detectors, the degeneracy between the distance D_L and the inclination of the GW measurement² (Eqs. 2 and 3) results in a face-on or face-off binary far away, which has a similar gravitational-wave amplitude to that of a close edge-on binary. This degeneracy contaminates the precision of the distance measurement. For simplicity, we use the geometrized unit system where $c = G = 1$.

$$h_+ = \frac{2M_z^{5/3} [\pi f(t)]^{2/3}}{D_L} [1 + (\hat{L} \cdot \hat{n})^2] \cos[\Phi(t)] \tag{2}$$

$$h_\times = \frac{4M_z^{5/3} [\pi f(t)]^{2/3} (\hat{L} \cdot \hat{n})}{D_L} \sin[\Phi(t)] \tag{3}$$

where h_+ and h_\times are the strengths of the GW signal of two different polarizations, M_z is the redshifted chirp mass, f is the wave frequency, Φ is the phase of GW, \hat{L} is the unit vector of the source’s angular momentum, and \hat{n} is the unit vector pointing to the direction of the source. Taking into account more standard sirens, it leads to a $N^{-1/2}$ convergence to the uncertainty of the Hubble constant, where N is the number of binary neutron-star mergers²³. It is predicted that, when more standard sirens are detected and another ground-based detector joins the network, the fractional uncertainty of the Hubble constant determined by the ground-based GW detectors will reach 2% within 5 years⁶.

This result is slightly better than that of the standard candle method.¹⁹

A space-borne GW antenna such as LISA and Taiji can avoid the degeneracy problem by virtue of its orbital motion. (For a detailed discussion of the orbital configuration for the space-borne antenna, please refer to refs. 9–11.) When a space-borne GW antenna is orbiting around the sun, the position and the orientation of the source relative to the antenna are gradually changing. The motion of the detector thus modulates the measured signal and its modulation depends on the position and the orientation of the source. As a result, the distance and the inclination of a GW source are no longer degenerate^{2,8}. This reduction in ambiguity increases the space antenna’s ability to determine the luminosity distance.

For instance, let us assume a binary black hole GW source is randomly distributed in the universe, its redshift is not >1 , and its total mass is $<10^6$ solar masses. Then, there is a 90% likelihood that an individual space antenna can localize the GW source with an error given by $\delta D_L/D_L < 8\%$ for the fractional distance and $\delta\Omega < 4 \text{ deg}^2$ for the orientation^{2,14,15}. For an individual antenna, without the EM counterparts of a GW source, the entanglement between the luminosity distance and the orientation will limit the precision to determine the distance^{2,8}. The fractional distance precision will be improved dramatically if the sky position of that GW source can be pinpointed. Considering the same type of GW sources discussed above, the distance error can be greatly reduced to 0.5% when the correlation between the distance and the orientation is combined². One way to pinpoint the GW source is to find its EM counterpart^{24,25}. Due to the poor understanding of the relation between the binary black hole merger GW event and its EM counterpart, it becomes difficult to find the EM counterpart either in advance or simultaneously²⁶.

Determining the Hubble constant with LISA-Taiji network

It was recently calculated that by the LISA–Taiji network, the localization of GW sources can be improved significantly without an EM counterpart¹⁵. Taking the above example, the orientation uncertainty of such a GW source can be reduced to $\delta\Omega < 0.005 \text{ deg}^2$. Consequently, the fractional distance precision will be improved to $\delta D_L/D_L < 0.5\%$. However, the EM counterpart is still important, as it can provide a redshift that is essential to calculate the Hubble constant. With such precise localization of a GW source, it will be relatively easy to discover its counterpart galaxy. The distributed density of a counterpart galaxy can be expressed as^{27,28}

$$\frac{dN}{dR d\Omega} \propto R \exp \left[\left(\frac{R}{R_*} \right)^{-4} \right] \tag{4}$$

with R as the co-moving distance and R_* as the Hubble distance. If we only consider a small redshift such as $z < 1$, the exponential part of Eq. (4) will always be ~ 1 . The projected number density $dN/d\Omega$ is ~ 300 galaxies/arcmin² given by the Hubble Deep Field²⁹. We can normalize Eq. (4) by integrating it into projected number density, which should be <300 galaxies/arcmin². Then, we have

$$\frac{dN}{dR d\Omega} < \frac{600 \cdot R}{R_0^2} \text{ galaxies/arcmin}^2 \tag{5}$$

where R_0 is the distance at $z = 1$. By assuming a cosmological model, we can convert the measured luminosity distance and its error to any other desired cosmic distance measure. By multiplying Eq. (5) with the GW error cube, the number of galaxies within the error cube can be derived. With $\delta\Omega < 0.005 \text{ deg}^2$ and $\delta D_L/D_L < 0.5\%$, the number of candidate host galaxies for a GW source with $z < 1$ is no >54 . According to the redshift-apparent

magnitude relation, the apparent magnitude of galaxies at distance $z = 1$ is between 24 and 25. Typically, for the spectroscopic measurement, the limiting magnitude for the device should be 3–4 magnitude greater, say 27–29, which challenges all the existing telescopes. Fortunately, future telescope such as LSST and WFIRST, assuming 2 years observation, could reach limiting magnitude of 27 and 29, respectively^{30,31}. Thus, all the candidate galaxies could be traced by a fiber spectrograph on an LSST-like or WFIRST-like telescope. With such a lower number, it is probable that an EM event is correlated with a GW event. In some particular cases, the spin-induced precession effects may allow certain degeneracy to be broken and the analysis can achieve 1 arcmin^{-2} pointing accuracy³². In such cases, the number of candidate galaxies can be reduced to a few. Thus, we can technically identify the counterpart galaxy of the GW source. Once the host galaxy of the GW source is identified, the redshift can be determined by the EM observation. With the distance of a GW source measured, the uncertainty of the Hubble constant $\delta H_0/H_0$ will now be $<0.5\%$.

Towards LISA–Taiji network

The LISA–Taiji network requires at least a 1-year overlap to realize the above purpose, which means Taiji needs to advance its schedule to match LISA’s availability to collect data. As the pioneer, LISA pathfinder has been launched in 2015. The mission is a technology demonstration and has achieved great success³³. LISA pathfinder has paved the way for the full LISA³⁴ project, which will start operating in orbit ~2032–2034. Taiji, the Chinese spaceborne GW detection mission, which has a heliocentric orbit similar to LISA, has established a three-step plan to launch in early 2030s.

Thus, it will have an overlap with LISA’s operating time^{12,13}. The first step has been accomplished by launching a pilot study satellite known as Taiji-1 satellite in 2019. The second step is to launch the Taiji pathfinder (also called Taiji-2) no later than 2025. Taiji-2 consists of two satellites, which are planned to demonstrate most technology of Taiji and to pave the way for the full Taiji project. The final step is to launch Taiji, which is similar to the LISA constellation in 2030s. Taiji (also called Taiji-3) consists of three identical satellites. The distance between the different pairs of two satellites is three million kilometers^{12,13}.

Taiji pathfinder, consists of two satellites, will be equipped with more technology related to the inter-satellite laser link compared to LISA pathfinder. The high technical requirement makes the Taiji pathfinder challenging¹³. As a completely new mission in this field, directly launching Taiji-2 seems to be a quite risky task. Thus, a pilot study satellite mission Taiji-1 was approved in 2018 not only to prepare the necessary technology for Taiji-2 but also to verify the performance capability of Taiji mission. Taiji-1 also serves as a benchmark to testify the feasibility of Taiji’s three-step plan.

Taiji-1, the first step of China’s efforts

Approved on 30 August 2018 and set to fly on 31 August 2019, Taiji-1, a 180 kg satellite, was a successful and quick mission. The orbit of Taiji-1 was a circular Sun-synchronous dawn/dusk orbit that was inclined at an angle of 97.69 deg. The orbit provided a relatively stable sun-facing angle, which ensured that the battery could always be constantly charged and that the temperature of the satellite should not fluctuate drastically. The orbit altitude was chosen to be 600 km, a tradeoff between the launching costs and the air drag. Similar to LISA pathfinder³³, two major technology units were tested on Taiji-1: the optical metrology system³⁵ and the drag-free control system³⁶. Due to the short-term development circle and the limited budget, the payload design was highly

simplified (Fig. 1a, b). The optical metrology system consisted of an optical bench, a phasemeter and two laser sources. The drag-free control system was composed of a gravitational reference sensor (GRS) (it consisted of both a sensor head and the corresponding sensor electronics), a drag-free controller, and two types of micro-propulsion systems. Figure 1 shows the distribution of the payload in Taiji-1.

Taiji-1 used two Nd-YAG lasers (first and second laser in Fig. 1a) with a wavelength of 1064.5 nm. Only one laser was working during the measurement process. The optical metrology system could switch one laser to the other under the command. The two laser beams were delivered to an optical bench by two fiber couplers (Fig. 1c). There was a frequency difference of ~1 kHz between the two delivered beams. Except for the reference interferometer, the optical bench contained two primary interferometers. The first was test mass interferometer (T.M. int.). One of the laser beams was aimed at a test mass and reflected to an optical bench (Fig. 1c). This unit measured the test mass motion. The other interferometer, called optical bench interferometer (O. B. int.), was used to monitor the optical bench noise. All of the interferometric beat notes were sensed and converted into sinusoidal voltages by the photodetectors. The phases of the sinusoidal voltages were decoded by the phasemeter³⁷.

By the data from the phasemeter, the precision of the two primary interferometers can be derived by $\delta L = \delta\phi \cdot \lambda \cdot (2\pi)^{-1/2}$, where δL is the precision of the interferometer, $\delta\phi$ denotes the phase noise of phasemeter data, and λ is the laser wavelength.

The GRS in Taiji-1, served as an accelerometer³⁸, is composed of a sensor head and the corresponding electronics. The sensor head consists of a cage and a test mass (Fig. 1c). The GRS has three axes, one nonsensitive axis and two sensitive axes (Fig. 1c). The nonsensitive axis points to the earth and the drag free is used along nonsensitive axis. The first sensitive axis is along flight direction.

By capacitive sensing, the GRS measured the disturbing acceleration of Taiji-1. The data were sent to a drag-free controller. The controller then commanded the thruster to exert forces to compensate the disturbing force experienced by Taiji-1. Two different types of thrusters were tested: a radio frequency ion thruster and a Hall effect thruster. Each type has four individual thrusters. They are assembled symmetrically on both sides of the satellite (Fig. 1a). These two types of thrusters, like the two lasers, backed up each other.

During the mission, all of the payloads were tested. All results fulfilled the mission requirement. Some of the measurements were shown in Fig. 2. For the T.M. int. and the O.B. int. (different lasers were used for each), the precision evaluated in the frequency band between 0.01 and 10 Hz was found to be $<1 \text{ nm Hz}^{-1/2}$. For some frequency bins, the precision could reach $25 \text{ pm Hz}^{-1/2}$ (Fig. 2a, b). The Taiji-1 GRS noise was taken from the second sensitive axis. The dynamic range of the second sensitive axis was $\pm 5.3 \times 10^{-5} \text{ m s}^{-2}$ and the acceleration noise of this axis measured by the readout voltage fluctuation was $10^{-10} \text{ m s}^{-2} \text{ Hz}^{-1/2}$ (Fig. 2c). The disturbance accelerations of the three axes of the Taiji-1 satellite readout by Taiji-1 GRS were shown in Fig. 2d. The nonsensitive axis was earth pointing, and the noise was mainly dominated by the GRS readout noise. While the first sensitive axis was along the flight direction, this noise was considered mainly caused by the air drag. The second sensitive axis was the orbit plane normal direction, and the acceleration measured by the GRS was $<2 \times 10^{-9} \text{ m s}^{-2} \text{ Hz}^{-1/2}$. The noise of both thrusters measured by the GRS was found to be $<1 \mu\text{N Hz}^{-1/2}$ (Fig. 2e) which was believed to be dominated by the GRS readout noise. The noise of the thrusters could also be calibrated by the data of the ion acceleration voltage, gas pressure at the supply valve,

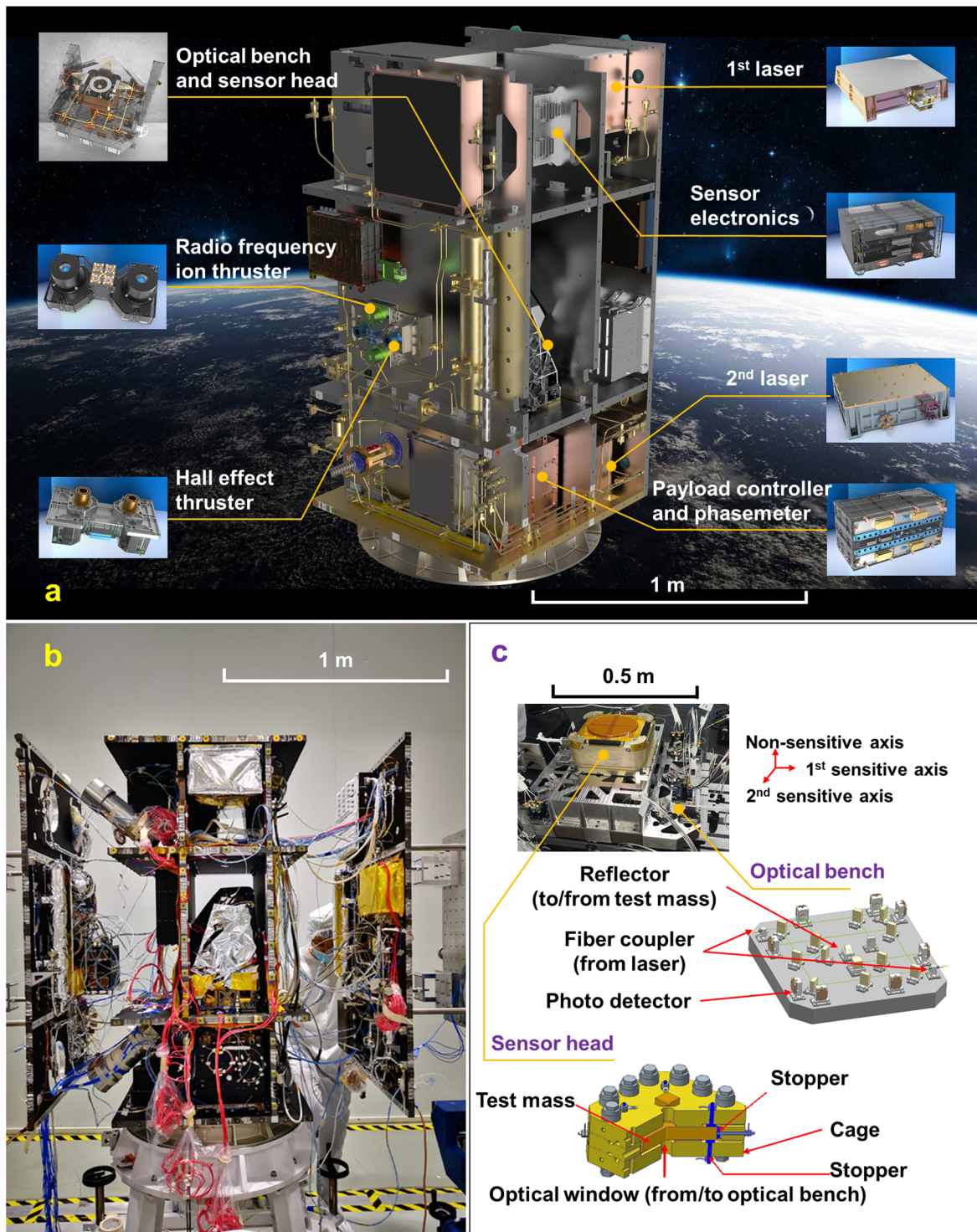


Fig. 1 Anatomy of Taiji-1 and its payloads. **a** The distribution of the payloads in Taiji-1. The optical bench and the sensor head are integrated in order to ensure the laser beam to get accurate access to the test mass. The difference between the nominal geometric center of the test mass and the mass center of the satellite is smaller than 0.15 mm after the balancing is achieved with a 0.1 mm measurement accuracy. **b** Taiji-1 satellite before assembling. **c** The core measurement unit. It contains an optical bench and a sensor head. The plate of the optical bench is made of invar steel, and the mirrors are made of fused silica. The cage of the sensor head is made of the low thermal expansion glass ceramics, and is coated with gold. The test mass is also coated with gold and is made of titanium alloy. The stoppers are used to prevent the test mass from contacting the inner surface of the cage during launch.

and the temperature around the thruster. By this method, the true thruster noise of the radio frequency ion thruster was derived as $\sim 0.15 \mu\text{N Hz}^{-1/2}$ (Fig. 2e).

A drag-free control experiment was also performed along the nonsensitive axis of the GRS. We used the thrusters on one side to

exert a sinusoidal force (the modulated peak in Fig. 2f), and the feedback controlled the thruster on the other side to compensate. The respective spectra densities were shown in Fig. 2f. The sinusoidal force (the modulated peak in Fig. 2f.) was well suppressed by using drag-free control, and the residue acceleration of

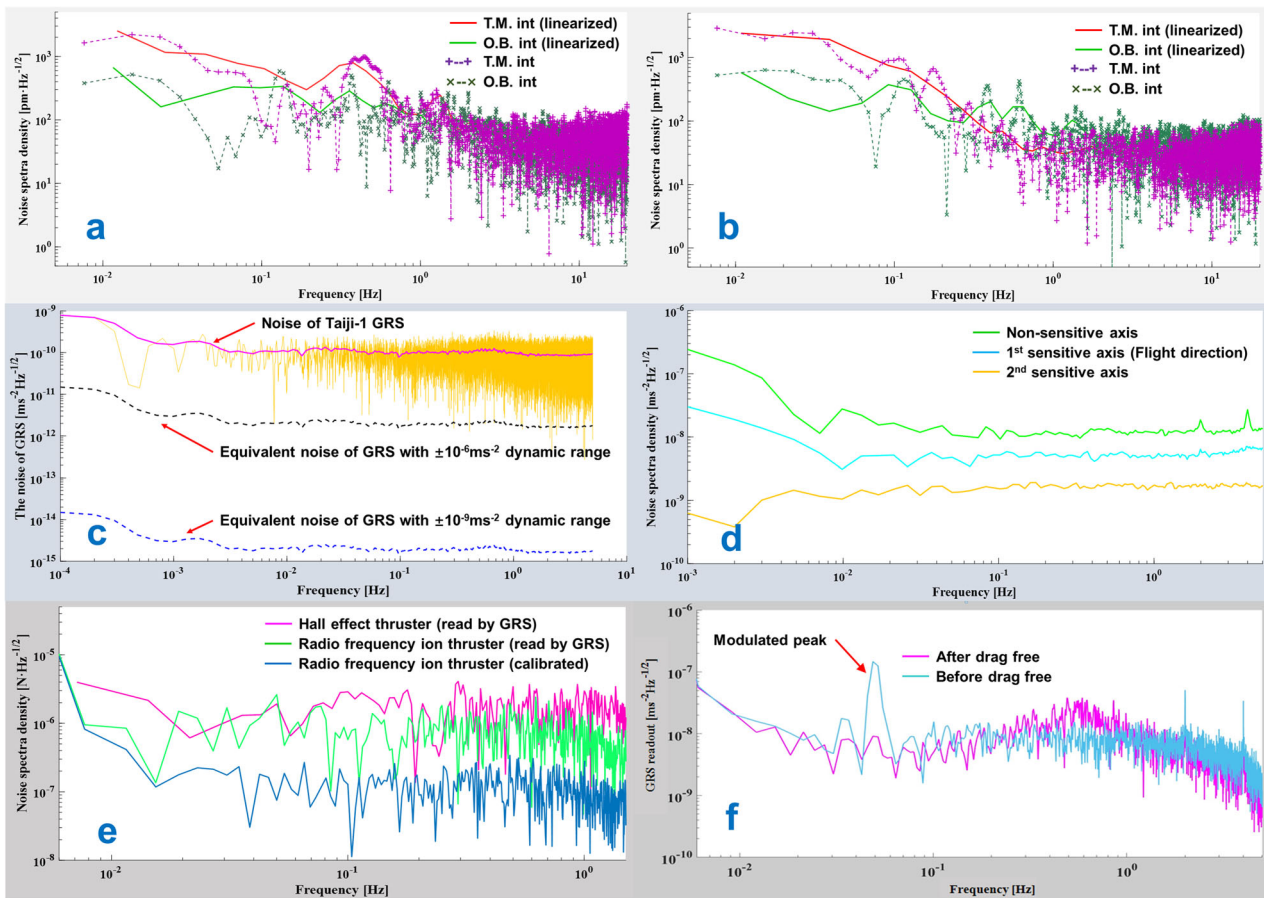


Fig. 2 On-orbit test results of Taiji-1 payload. **a** The precision of optical bench interferometer (O.B. int) and test mass interferometer (T.M. int) by using the first laser. **b** The precision of the two primary interferometers (using second laser). **c** The noise of Taiji-1’s gravitational reference sensor (GRS) and the equivalent noise of the GRS corresponding to smaller dynamic ranges. **d** The acceleration of the Taiji-1 satellite in three axes readout by GRS. **e** The noise from the two types of thrusters readout by the GRS and the calibrated noise of the radio frequency ion thruster. **f** The gravitational wave readout in spectrum density before and after the drag-free control.

the satellite was $<10^{-8} \text{ m s}^{-2} \text{ Hz}^{-1/2}$. The stability of the temperature control was $\sim \pm 2.6 \text{ mK}$. A more detailed analysis of Taiji-1 payload testing and the improved results would be presented in a special issue to be published soon.

The GRS noise induced by the voltage fluctuation is always proportional to its dynamic range³⁹ (Eqs. 6 and 7), where S is the area of the capacitor plate, m is the mass of test mass, d is the distance of the capacitor, V_p is the preload voltage of the capacitor, V_r is the readout voltage, δV_p is the preload voltage noise, δV_r is the readout voltage noise, and ϵ_0 is electrostatic constant.

$$\text{GRS readout acceleration : } A_{\text{readout}} = \frac{2\epsilon_0 S}{md^2} V_p V_r \quad (6)$$

$$\text{GRS Acceleration noise : } \delta a = \frac{2\epsilon_0 S}{md^2} V_p V_r \left(\frac{\delta V_p}{V_p} + \frac{\delta V_r}{V_r} \right) \quad (7)$$

It is obvious that reducing the dynamic range of GRS will in turn reduce the GRS acceleration noise (Fig. 2c).

To summarize, the first on-orbit scientific run of Taiji-1 showed that the space-borne interferometers could work properly, the distance measurement noise amplitude spectra density of O.B. interferometer was at the level of $100 \text{ pm Hz}^{-1/2}$ ($10 \text{ mHz} - 1 \text{ Hz}$). In some higher frequency bin, it approached $25 \text{ pm Hz}^{-1/2}$. The performance of GRS also fulfilled the requirement, with the evaluated acceleration measurement noise amplitude spectra density being $10^{-10} \text{ m s}^{-2} \text{ Hz}^{-1/2}$. The noise amplitude spectra

density of the thruster exerting force was calibrated to be $<0.15 \text{ } \mu\text{N Hz}^{-1/2}$. The residue acceleration of the satellite after the drag free was $<1 \times 10^{-8} \text{ m s}^{-2} \text{ Hz}^{-1/2}$. The on-orbit performance of Taiji-1 demonstrated the feasibility of the payloads. The design, the manufacturing, the assembling, and the adjusting of payloads were effectively verified.

Outlook

A new frontier was depicted above that the data of LISA–Taiji network can be used to study the cosmology in a more precise manner. The searching for GW signals with space-borne detectors network will help us to understand not only the nature of gravity but also the expanding history of our universe. However, a few technology challenges faced by LISA and Taiji are still needed to be tackled in near future.

The successful flight of Taiji-1 has verified the feasibility of the three-step plan of Taiji. Encouraged by the achievement of Taiji-1, the Taiji scientific collaboration is looking forward to flying Taiji in early 2030s. It is our optimistic expectation that LISA and Taiji will be both orbiting the sun to detect a standard siren from a massive binary black hole merger. With the LISA–Taiji network, it is highly possible that the Hubble constant can be determined with an uncertainty $<0.5\%$.

Data availability

The data that support the findings of this study are available from the authors on reasonable request, see Author contributions for specific data sets.

Received: 21 August 2020; Accepted: 14 January 2021;

Published online: 24 February 2021

References

- Schutz, B. F. Determining the Hubble constant from gravitational wave observations. *Nature* **323**, 310–311 (1986).
- Holz, D. E. & Hughes, S. A. Using gravitational-wave standard sirens. *Astrophys. J.* **629**, 15–22 (2005).
- The LIGO Scientific Collaboration and The Virgo Collaboration, The 1M2H Collaboration, The Dark Energy Camera GW-EMCollaboration and the DES Collaboration, The DLT40 Collaboration, The Las Cumbres Observatory Collaboration, The VINRO UGE Collaboration & The MASTER Collaboration. A gravitational-wave standard siren measurement of the Hubble constant. *Nature* **551**, 85–88 (2017).
- The LIGO Scientific Collaboration. Advanced LIGO. *Class. Quantum Gravity* **32**, 074001 (2015).
- The Virgo Scientific Collaboration. Advanced Virgo: a second-generation interferometric gravitational wave detector. *Class. Quantum Gravity* **32**, 024001 (2015).
- Chen, H., Fishbach, M. & Holz, D. E. A two per cent Hubble constant measurement from standard sirens within five years. *Nature* **562**, 545–547 (2018).
- Anand, S. et al. Optical follow-up of the neutron star-black hole mergers S200105ae and S200115j. *Nat. Astron.* **5**, 46–53 (2021).
- Amaro-Seoane, P. et al. Laser interferometer space antenna. Preprint at <https://arxiv.org/ftp/arxiv/papers/1702/1702.00786.pdf> (2017).
- Bender, P. et al. *LISA Pre-Phase A Report* (Max-Planck-Institut für Quantenoptik, 1998).
- Cyranoski, D. Chinese gravitational-wave hunt hits crunch time. *Nature* **531**, 150–151 (2016).
- Hu, W. R. & Wu, Y. L. The Taiji Program in Space for gravitational wave physics and the nature of gravity. *Natl Sci. Rev.* **4**, 685–686 (2017).
- Luo, Z. R., Guo, Z. K., Jin, G., Wu, Y. L. & Hu, W. R. A brief analysis to Taiji: science and technology. *Results Phys.* **16**, 102918 (2020).
- Luo, Z. R., Jin, G., Wu, Y. L. & Hu, W. R. The Taiji program: a concise overview. *Progr. Theor. Exp. Phys.* <https://doi.org/10.1093/ptep/ptaa083> (2020).
- Cutler, C. Angular resolution of the LISA gravitational wave detector. *Phys. Rev. D* **57**, 7089 (1998).
- Ruan, W., Liu, C., Guo, Z., Wu, Y. & Cai, R. The LISA–Taiji network. *Nat. Astron.* **4**, 108–109 (2020).
- Hubble, E. A relation between distance and radial velocity among extragalactic nebulae. *Proc. Natl Acad. Sci. USA* **15**, 169 (1929).
- Lemaître, E. The beginning of the world from the viewpoint of quantum theory. *Nature* **127**, 706 (1931).
- Freedman, Wendy L. & Madore, Barry F. The Hubble constant. *Annu. Rev. Astron. Astrophys.* **48**, 673–710 (2010).
- Riess, A. G., Casertano, S., Yuan, W., Macri, L. M. & Scolnic, D. Large magellanic cloud cepheid standards provide a 1% foundation for the determination of the hubble constant and stronger evidence for physics beyond Λ CDM. *Astrophys. J.* **876**, 85 (2019).
- Planck Collaboration, Planck 2018 results. VI. Cosmological parameters. *A&A* **641**, A6 (2020).
- Abbott, B. P. et al. GW170817: observation of gravitational waves from a binary neutron star inspiral. *Phys. Rev. Lett.* **119**, 161101 (2017).
- Abbott, B. P. et al. Multi-messenger observations of a binary neutron star merger. *Astrophys. J.* **848**, L12 (2017).
- Hirata, C. M., Holz, D. E. & Cutler, C. Reducing the weak lensing noise for the gravitational wave Hubble diagram using the non-Gaussianity of the magnification distribution. *Phys. Rev. D.* **81**, 124046 (2010).
- Begelman, M., Blandford, R. & Rees, M. Massive black hole binaries in active galactic nuclei. *Nature* **287**, 307–309 (1980).
- Dotti, M., Colpi, M., Haardt, F. & Mayer, L. Supermassive black hole binaries in gaseous and stellar circumnuclear discs: orbital dynamics and gas accretion. *Mon. Not. R. Astron. Soc.* **379**, 956–962 (2007).
- Graham, M. J. et al. Candidate electromagnetic counterpart to the binary black hole merger gravitational-wave event S190521g. *Phys. Rev. Lett.* **124**, 251102 (2020).
- Kaiser, N. Weak gravitational lensing of distant galaxies. *ApJ* **388**, 272 (1992).
- Hu, W. Power spectrum tomography with weak lensing. *ApJ* **522**, L21 (1999).
- Williams, R. E. et al. The Hubble deep field: observations, data reduction, and galaxy photometry. *Astron. J.* **112**, 1335 (1996).
- LSST collaboration, LSST: from Science Drivers to Reference Design and Anticipated Data Products. *The Astrophysical Journal*, **873**, 111 (2019).
- The WFIRST Deep Field Working Group & WFIRST Science Investigation Team Members and Community Members. LSST observations of WFIRST deep fields. Preprint at <https://arxiv.org/abs/astro-ph/1812.00514> (2018).
- Vecchio, A. LISA observations of rapidly spinning massive black hole binary systems. *Phys. Rev. D* **70**, 042001 (2004).
- Armano, M. et al. Sub-femto-g free fall for space-based gravitational wave observatories: LISA pathfinder results. *Phys. Rev. Lett.* **116**, 231101 (2016).
- Wanner, G. Space-based gravitational wave detection and how LISA Pathfinder successfully paved the way. *Nat. Phys.* **15**, 200–202 (2019).
- Heather, E. A. LISA Pathfinder: Optical Metrology System monitoring during operations. *J. Phys.* **840**, 012034 (2017).
- Fichter, W., Gath, P., Vitale, S. & Bortoluzzi, D. LISA Pathfinder drag-free control and system implications. *Class. Quantum Gravity* **22**, S139–S148 (2005).
- Gerberding, O. et al. Phasemeter core for intersatellite laser heterodyne interferometry: modelling, simulations and experiments. *Class. Quantum Gravity* **30**, 235029 (2013).
- Touboul, P., Willemonot, E., Foulon, B. & Josselin, V. Accelerometers for CHAMP, GRACE and GOCE space missions: synergy and evolution. *Boll. Geof. Teor. Appl.* **40**, 321–327 (1999).
- Josselin, V., Touboul, P. & Kielbasa, R. Capacitive detection scheme for space accelerometers applications. *Sens. Actuators* **78**, 92–98 (1999).

Acknowledgements

This work is supported by the “Strategic Priority Research Program of the Chinese Academy of Science” (XDA15020709, XDB23030000).

Author contributions

Taiji Scientific Collaboration contributed to the work presented in this paper.

Competing interests

The authors declare no competing interests.

Additional information

Supplementary information The online version contains supplementary material available at <https://doi.org/10.1038/s42005-021-00529-z>.

Correspondence and requests for materials should be addressed to Y.-L.W., Z.-R.L. or J.-Y.W.

Reprints and permission information is available at <http://www.nature.com/reprints>

Publisher’s note Springer Nature remains neutral with regard to jurisdictional claims in published maps and institutional affiliations.



Open Access This article is licensed under a Creative Commons Attribution 4.0 International License, which permits use, sharing, adaptation, distribution and reproduction in any medium or format, as long as you give appropriate credit to the original author(s) and the source, provide a link to the Creative Commons license, and indicate if changes were made. The images or other third party material in this article are included in the article’s Creative Commons license, unless indicated otherwise in a credit line to the material. If material is not included in the article’s Creative Commons license and your intended use is not permitted by statutory regulation or exceeds the permitted use, you will need to obtain permission directly from the copyright holder. To view a copy of this license, visit <http://creativecommons.org/licenses/by/4.0/>.

© The Author(s) 2021

The Taiji Scientific Collaboration

Yue-Liang Wu^{1,2,3,4,5}✉, Zi-Ren Luo^{1,2,5}✉, Jian-Yu Wang^{1,5,6}✉, Meng Bai⁷, Wei Bian^{1,5,7}, Rong-Gen Cai^{1,3,5}, Zhi-Ming Cai⁸, Jin Cao⁸, Di-Jun Chen^{5,9}, Ling Chen⁷, Li-Sheng Chen¹⁰, Ming-Wei Chen^{1,2}, Wei-Biao Chen^{5,9}, Ze-Yi Chen⁹, Lin-Xiao Cong¹, Jian-Feng Deng⁸, Xiao-Long Dong⁷, Li Duan^{1,2}, Sen-Quan Fan⁸, Shou-Shan Fan¹¹, Chao Fang¹², Yuan Fang⁸, Ke Feng¹³, Pan Feng⁹, Zhun Feng⁷, Rui-Hong Gao^{1,2}, Run-Lian Gao⁷, Zong-Kuan Guo^{1,3,5}, Jian-Wu He^{1,2}, Ji-Bo He¹ , Xia Hou⁹, Liang Hu², Wen-Rui Hu^{1,2}, Zhi-Qiang Hu¹ , Min-Jie Huang⁹, Jian-Jun Jia^{1,5,6}, Kai-Li Jiang¹¹, Gang Jin^{2,5}, Hong-Bo Jin¹⁴, Qi Kang^{1,2}, Jun-Gang Lei¹⁵, Bo-Quan Li⁷, Dong-Jing Li¹², Fan Li⁷, Hao-Si Li², Hua-Wang Li⁸, Liu-Feng Li¹⁰, Wei Li¹², Xiao-Kang Li^{1,2}, Ying-Min Li¹ , Yong-Gui Li¹, Yun-Peng Li¹⁵, Yu-Peng Li^{1,12}, Zhe Li¹², Zhi-Yong Lin¹, Chang Liu¹ , Dong-Bin Liu¹², He-Shan Liu^{2,5}, Hong Liu⁸, Peng Liu¹¹, Yu-Rong Liu⁷, Zong-Yu Lu¹⁰, Hong-Wei Luo⁹, Fu-Li Ma⁷, Long-Fei Ma^{1,2}, Xiao-Shan Ma⁷, Xin Ma⁷, Yi-Chuan Man⁷, Jian Min¹⁵, Yu Niu^{1,2}, Jian-Kang Peng¹⁰, Xiao-Dong Peng⁷, Ke-Qi Qi¹², Li-É Qiang⁷, Cong-Feng Qiao¹ , Ye-Xi Qu⁹, Wen-Hong Ruan¹ , Wei Sha¹², Jia Shen^{1,2}, Xing-Jian Shi⁸, Rong Shu⁶, Ju Su⁷, Yan-Lin Sui¹², Guang-Wei Sun⁹, Wen-Lin Tang⁷, Hong-Jiang Tao¹², Wen-Ze Tao¹⁵, Zheng Tian⁷, Ling-Feng Wan¹⁰, Chen-Yu Wang^{1,2}, Jia Wang², Juan Wang^{1,2}, Lin-Lin Wang⁷, Shao-Xin Wang¹², Xiao-Peng Wang¹², Yu-Kun Wang¹², Zhi Wang^{1,12}, Zuo-Lei Wang¹⁵, Yu-Xiao Wei¹, Di Wu², Li-Ming Wu¹, Peng-Zhan Wu¹⁶, Zhi-Hua Wu⁸, Dong-Xue Xi¹⁵, Yi-Fang Xie⁷, Guo-Feng Xin⁹, Lu-Xiang Xu^{1,5,17}, Peng Xu^{1,16}, Shu-Yan Xu^{5,17}, Yu Xu⁸, Sen-Wen Xue^{1,2}, Zhang-Bin Xue⁷, Chao Yang^{1,2}, Ran Yang^{1,2}, Shi-Jia Yang¹⁵, Shuang Yang⁷, Yong Yang⁸, Zhong-Guo Yang⁹, Yong-Li Yin¹⁸, Jin-Pei Yu⁸, Tao Yu¹², Ài-Bing Zhang⁷, Chu Zhang^{1,2}, Min Zhang^{1,4,5}, Xue-Quan Zhang⁷, Yuan-Zhong Zhang³, Jian Zhao⁹, Wei-Wei Zhao⁸, Ya Zhao^{1,12}, Jian-Hua Zheng⁷, Cui-Yun Zhou⁹, Zhen-Cai Zhu⁸, Xiao-Bo Zou¹⁶ & Zi-Ming Zou⁷

¹Taiji Laboratory for Gravitational Wave Universe (Beijing/Hangzhou), University of Chinese Academy of Sciences (UCAS), Beijing, China.

²National Microgravity Laboratory, Center for Gravitational Wave Experiment, Institute of Mechanics, Chinese Academy of Sciences (CAS), Beijing, China. ³Institute of Theoretical Physics, Chinese Academy of Sciences, Beijing, China. ⁴International Centre for Theoretical Physics Asia-Pacific (ICTP-AP) (Beijing/Hangzhou), UCAS, Beijing, China. ⁵Hangzhou Institute for Advanced Study, UCAS, Hangzhou, China. ⁶Shanghai Institute of Technical Physics, CAS, Shanghai, China. ⁷National Space Science Center, CAS, Beijing, China. ⁸Innovation Academy for Microsatellites, CAS, Shanghai, China. ⁹Space Laser Engineering Technology Laboratory, Shanghai Institute of Optics and Fine Mechanics, CAS, Shanghai, China. ¹⁰Innovation Academy for Precision Measurement Science and Technology, CAS, Wuhan, China. ¹¹Tsinghua University, Beijing, China. ¹²Changchun Institute of Optics, Fine Mechanics and Physics, CAS, Changchun, China. ¹³Aerospace Information Research Institute, CAS, Beijing, China. ¹⁴Nation Astronomical Observatory, CAS, Beijing, China. ¹⁵Lanzhou Institute of Physics, Lanzhou, China. ¹⁶Lanzhou University, Lanzhou, China. ¹⁷Nanyang Technological University, Singapore, Singapore. ¹⁸China Astronaut Research and Training Center, Beijing, China.

✉email: ylwu@mail.itp.ac.cn; luoziren@imech.ac.cn; jywang@mail.sitp.ac.cn